Isotopic decoupling of K from Sr and Nd in the Saima alkaline complex, NE China: interactions of cratonic roots and asthenosphere

Nan Gao[1,2], Yingkui Xu[1,3] 🔾, Dan Zhu[3,4], Yang Li[1,3], Xiongyao Li[1,3], Jianzhong Liu[1,3] and Jin-Cheng Luo[4]

[1]Centre for Lunar and Planetary Sciences, Institute of Geochemistry, Chinese Academy of Sciences, Guiyang 550081, China; [2]University of Chinese Academy of Sciences, Beijing 100049, China; [3]CAS Centre for Excellence in Comparative Planetology, Hefei 230026, China and [4]State Key Laboratory of Ore Deposit Geochemistry, Institute of Geochemistry, Chinese Academy of Sciences, Guiyang 550081, China

CAMBRIDGE
UNIVERSITY PRESS

Abstract

We report high-precision K isotopes, apatite U–Pb ages, whole-rock elements and Sr–Nd isotopes for the Saima nephelite syenite in the North China Craton. Trace-element and Sr–Nd–Hf–O isotope data indicate the presence of subducting sediments in the source region, while K isotopic compositions show a narrow range between –0.54 ‰ and –0.28 ‰, with an average of –0.41 ± 0.06 ‰, identical to the value of the asthenosphere. The nearly identical K isotopic compositions are low probability events compared with the K isotopic compositions of island arc lavas reported previously (–1.55 ‰ to +0.2 ‰). Although crustal contamination is consistent with the Sr–Nd–K isotopic data, alternatively we propose that the isotopic data also reconcile with the interaction between cratonic roots and the underlying convective asthenosphere, if this interaction is over prolonged periods of time. Numerical simulations successfully reproduced the observed data, if the metasomatism of the lithospheric mantle root, the source of the Saima alkaline rocks, occurred 500 Ma ago. Our study reveals that the isotopic compositions of fast-diffusion components in a lithospheric mantle metasomatized by ancient subducting melts can be effectively homogenized by convective asthenosphere through diffusion over a long time interval.

1. Introduction

Recent studies have shown that potassium isotopes are sensitive to crust–mantle interactions and can be used to trace deep potassium cycles (Sun *et al.* 2020; Hu *et al.* 2021*a*; Wang, Z.-Z. *et al.* 2021; Parendo *et al.* 2022). Orogenic high-potassium rocks and island arc lavas show large variations in K isotopic composition, indicating the mixing of mantle sources and subducted sediments. This is because the sediments display more variable K isotopic compositions, ranging from –1.31 ‰ to –0.02 ‰, while the mantle has a limited range of –0.42 ± 0.08 ‰ (two standard deviations (2 SD)) (Hu *et al.* 2021*b*). In addition to subducted sediment melts or fluids, metasomatized lithospheric mantle roots (MLMRs) are also affected by the asthenosphere (McKenzie, 1989). The creation of interstitial melts from the partial melting of MLMRs is consistent with modern physical observations that the lithosphere–asthenosphere boundary (LAB) is enriched in the melt (Naif *et al.* 2013; Debayle *et al.* 2020). Combined with the observation that the convective asthenosphere also contains a significant amount of melt (Kawakatsu *et al.* 2009; Debayle *et al.* 2020), the interaction between the MLMR and asthenosphere is the mass exchange of interstitial melts by chemical diffusion in these two reservoirs. Chemical diffusion tends to homogenize an initially inhomogeneous system in chemical and isotopic compositions (Lasaga, 1998; Zhang, 2008); thus, different elements with different diffusivities will show different extents of homogeneities within a given time span. Considering the fast diffusion rate of K compared with Sr and Nd (Behrens & Hahn, 2009; Zhang *et al.* 2010), the decoupling of K from the Sr and Nd isotopic compositions of the MLMR is expected if the interaction between the MLMR and asthenosphere is mainly controlled by chemical diffusion. However, this process has not been evaluated before.

Alkaline rocks derived from MLMRs can offer opportunities to investigate the interaction of MLMRs and the asthenosphere (Foley *et al.* 1987). The K, Sr and Nd isotopic compositions of alkaline rocks are similar to those of the subducted sediments (Wang, K. *et al.* 2021; Wang, Z.-Z. *et al.* 2021) and should be distinctly different from those of the asthenosphere, which has a limited K isotopic composition range at the initial stage (Hu *et al.* 2021*b*). Therefore, the isotopic compositions (K, Sr and Nd) of alkaline rocks derived from MLMRs are good proxies for evaluating the extent and nature of the interaction between the MLMR and asthenosphere. The Saima alkaline complex is situated on the northeastern margin of the North China Craton (NCC).

Previous studies have suggested that the Saima complex formed at 224 Ma, originating from the lithospheric mantle. The Saima alkaline rocks have heterogeneous initial $^{87}Sr/^{86}Sr$ ratios (0.7072 to 0.7089), low $\epsilon_{Nd}(t)$ (−11.3 to −13), extremely negative zircon $\epsilon_{Hf}(t)$ (−11 to −14) and elevated $\delta^{18}O$ (+7.1 ‰ to +8.4 ‰) values, indicating their mantle source was metasomatized by melts derived from subducted sediments (Zhu *et al.* 2016, 2017). Therefore, in this study, we report high-precision K isotopes, apatite U–Pb ages, whole-rock elements and Sr–Nd isotopes of the Saima alkaline rocks and perform numerical simulations to evaluate the extent of interaction between the lithospheric and asthenospheric mantle beneath the NCC.

2. Methods

2.a. Apatite U–Pb dating

Apatite U–Pb dating was performed on an Analytik-Jena M90 quadrupole inductively coupled plasma mass spectrometer (ICP-MS) with a 193 nm NWR193 Ar-F excimer laser at the State Key Laboratory of Ore Deposit Geochemistry, Institute of Geochemistry, Chinese Academy of Sciences, Guiyang, China. Apatite was sampled on 40-micron spots using a laser at 8 Hz and a density of ~4 J cm^{-2}. The data are provided in online Supplementary Material Table S1.

2.b. Whole-rock major- and trace-element analyses

The rock samples were crushed to 200 mesh. After drying at 105 °C for 4 h, the rock powders were treated to produce glass beads for analysis using X-ray fluorescence spectroscopy (XRF) at the ALS Laboratory Group, Analytical Chemistry and Testing Services, Guangzhou, China. The relative standard deviations of the major-element concentrations in repeat analyses were <5 %.

Whole-rock trace-element analyses were performed on an Agilent 7700e ICP-MS at Wuhan Sample Solution Analytical Technology, Wuhan, China. A solution of Rh was used as an internal standard to monitor signal drift during the analysis. The measured concentrations were calibrated against the AGV-2, BHVO-2, BCR-2 and RGM-2 standards. The precision during trace-element analysis was generally better than 5 %. The major- and trace-element data are listed in online Supplementary Material Table S2.

2.c. Whole-rock Sr–Nd isotope analyses

Strontium and Nd isotopic analyses were carried out at the State Key Laboratory of Isotope Geochemistry, GIGCAS. Approximately 100 mg of sample powder were dissolved in HF + HNO$_3$ acid in Teflon bombs at ~195 °C for two days. Sr, Nd and rare earth elements (REEs) were separated by applying cation columns; Nd was further separated using HDEHP-coated Kef columns. Sr and Nd isotopic analyses were completed using a Micromass Isoprobe multi-collector (MC)-ICP-MS. To correct for mass fractionation, the measured Sr and Nd isotope ratios were normalized to $^{86}Sr/^{88}Sr = 0.1194$ and $^{146}Nd/^{144}Nd = 0.7219$. Isotopic compositions and calculated initial $^{87}Sr/^{86}Sr$ and $\epsilon_{Nd}(t)$ values are listed in online Supplementary Material Table S3.

2.d. Whole-rock K isotope analyses

Potassium isotopic analyses were performed at the Isotope Laboratory at the University of Washington, Seattle. In addition to samples of the nephelite syenites, a USGS rock standard (G-2) was also processed and analysed to assess the accuracy and reproducibility of our analytical procedure. Approximately 1–8 mg of rock powder were digested with a concentrated HF-HNO$_3$ acid mixture and heated on a hotplate until complete dissolution. The dissolved samples were then fully dried under heat lamps and redissolved in 0.5 N HNO$_3$. Following the previous purification procedure (Xu *et al.* 2019), samples were passed twice through column chemistry with Bio-Rad AG 50 W-X8 cation exchange resin (200–400 mesh) in 0.5 N HNO$_3$ media to separate K from other elements. The purified K solution was dried and dissolved in 3 % HNO$_3$ for instrumental analysis. Potassium isotopic ratios were measured by the sample-standard bracketing method using a Nu Plasma II MC-ICP-MS and are reported in standard delta (δ) notation relative to NIST SRM 3141a (Hu *et al.* 2018), that is, $\delta^{41}K$ (‰) = (($^{41}K/^{39}K)_{sample}/(^{41}K/^{39}K)_{NIST\ SRM\ 3141a} − 1) \times 1000$. The long-term external precision based on the replicate analysis of geo-standards and seawater samples was <0.06 ‰ (95 % confidence interval (c.i.)). G-2 yielded $\delta^{41}K$ values of −0.47 ± 0.04 ‰ (95 % c.i., N = 10) within the uncertainty of previously published data (Xu *et al.* 2019). The data are listed in Table 1.

3. Results and discussion

3.a. K–Sr–Nd isotopic compositions of samples

Apatite U–Pb dating results showed that the syenites formed at 236 ± 55 Ma (MSWD = 1.07) (online Supplementary Material Fig. S1). The Saima syenites have relatively high initial $^{87}Sr/^{86}Sr$ ratios (0.7085 to 0.7087) and low $^{143}Nd/^{144}Nd$ ratios (0.511709 to 0.511719) (online Supplementary Material Fig. S2) at an intrusion age of 230 Ma, indicating the involvement of crustal material during magma ascent or in the source region (Hawkesworth & Vollmer, 1979; Jahn *et al.* 1999). Except for one sample ($\delta^{41}K = -0.14 ± 0.09$ ‰), K isotopic compositions of the Saima nephelite syenites display a restricted range between −0.54 ‰ and −0.28 ‰, with an average of −0.41 ± 0.06 ‰ (2 SD; Fig. 1; Table 1), suggesting a mantle-like K isotopic composition. Evidently, K isotopes decoupled from the Sr–Nd isotope system for the Saima alkaline complex in the northeastern NCC. To investigate why the isotopes were decoupled, the influence of the magma evolution process, e.g. magma differentiation and crust contamination, should first be evaluated.

All samples of the Saima nephelite syenites are highly enriched in light rare earth elements (LREEs) and large ion lithophile elements (LILEs) compared to OIB and E-MORB (Sun & McDonough, 1989), showing a distribution pattern like that of UCC (Rudnick & Gao, 2014) (online Supplementary Material Fig. S3), which indicates the involvement of crustal material. No significant correlations were observed in the I_{Sr}–1/Sr and I_{Sr}–MgO plots (online Supplementary Material Fig. S4), indicating that crustal contamination was not significant during magma ascent. The simple binary mixing simulation results showed that the degree of contamination was low, at ~3 % (online Supplementary Material Fig. S2), suggesting that crustal material mixing into the source region was derived from subducting melts. In addition, the lack of correlation between $\delta^{41}K$ and major elements (SiO$_2$, MgO and K$_2$O) or loss on ignition (LOI) (online Supplementary Material Fig. S5) indicates that there is no obvious K isotope fractionation in the process of magma differentiation and post-magmatic alteration, which is consistent with the findings of the previous research (Hu *et al.* 2021b). Therefore, the Saima alkaline rocks represent the original K–Sr–Nd isotope characteristics of the source region of the lithospheric mantle.

Table 1. Potassium isotopic compositions for the Saima nephelite syenites in northeastern China

Sample	Rock type	K$_2$O (wt %)	δ^{41}K (‰)	2SD (‰)*	95 % c.i. (‰)†	N‡
SM01	Nephelite syenite	11.55	−0.40	0.11	0.08	4
Replicate			−0.47	0.10	0.05	7
Average			−0.44	0.07	0.04	
SM02	Nephelite syenite	11.80	−0.44	0.07	0.03	7
SM03	Nephelite syenite	11.30	−0.47	0.04	0.02	6
SM04	Nephelite syenite	11.70	−0.37	0.09	0.05	6
SM05	Nephelite syenite	11.50	−0.38	0.10	0.05	6
SM06	Nephelite syenite	11.45	−0.39	0.07	0.04	6
SM07	Nephelite syenite	11.30	−0.46	0.06	0.03	5
SM08	Nephelite syenite	11.20	−0.35	0.08	0.05	5
SM09	Nephelite syenite	11.25	−0.38	0.03	0.02	6
SM10	Nephelite syenite	11.60	−0.39	0.07	0.04	6
SM11	Nephelite syenite	11.25	−0.33	0.06	0.03	7
SM12	Nephelite syenite	12.40	−0.49	0.08	0.05	5
SM20	Nephelite syenite	11.45	−0.28	0.10	0.06	5
Replicate			−0.34	0.07	0.04	6
Average			−0.32	0.06	0.03	
SM21	Nephelite syenite	12.55	−0.44	0.09	0.04	7
SM22	Nephelite syenite	12.70	−0.44	0.09	0.04	7
SM23	Nephelite syenite	11.90	−0.42	0.07	0.04	6
SM24	Nephelite syenite	11.55	−0.44	0.11	0.05	7
SM25	Nephelite syenite	11.90	−0.54	0.09	0.04	7
SM26	Nephelite syenite	11.90	−0.31	0.10	0.05	6
SM27	Nephelite syenite	12.60	−0.45	0.10	0.05	6
SM28	Nephelite syenite	11.85	−0.42	0.07	0.04	6
SM29	Nephelite syenite	11.80	−0.39	0.07	0.04	6
SM31	Nephelite syenite	11.75	−0.14	0.09	0.05	6
SM32	Nephelite syenite	12.60	−0.51	0.10	0.05	7
G–2	Granite, USGS		−0.46	0.08	0.10	3
Duplicate			−0.47	0.08	0.04	7

Note: *2SD = twice the standard deviation of the population of N repeat measurements of a sample solution; †95 % c.i. = 95 % confidence interval. The 95 % c.i. was corrected using the student t-factor (Platzner, 1997) and calculated from the 2SD of the sample measurements in the analytical session; ‡N = number of analyses.

3.b. Diffusion modelling of K–Sr–Nd in the interactions of cratonic roots and asthenosphere

The presence of partial melt at the LAB has been confirmed by simulations based on modern seismic and electromagnetic observations (Kawakatsu *et al.* 2009; Naif *et al.* 2013; Rychert *et al.* 2021). Besides facilitating plate motion, such melts beneath the lithospheric plates also interact with the lithospheric mantle and affect the composition of the lithosphere over a long time interval. Here, we propose that the initially metasomatized lithospheric mantle was later altered by chemical diffusion between melts at the LAB, and the difference in diffusion rates between K and Sr–Nd is the main factor for the isotope decoupling.

The Fuxian kimberlites formed at ~465 Ma and originated from subduction-related lithospheric mantle metasomatism in the eastern NCC (Zhang & Yang, 2007); thus, the enrichment events associated with their origin should have occurred earlier. Here, it is assumed that the metasomatism of K-rich melts occurred at ~500 Ma. Because of the close geographical location and similar geological background to the Fuxian kimberlites, it is assumed that the lithospheric mantle roots of the Saima alkaline complex were coevally metasomatized by K-rich melts at ~500 Ma, after which no further metasomatism events occurred. The relatively oxidized upper mantle can produce partial melts with different volatile (carbon, hydrogen) ratios, which efficiently extract highly incompatible elements. The interstitial melts enriched in volatiles (such as
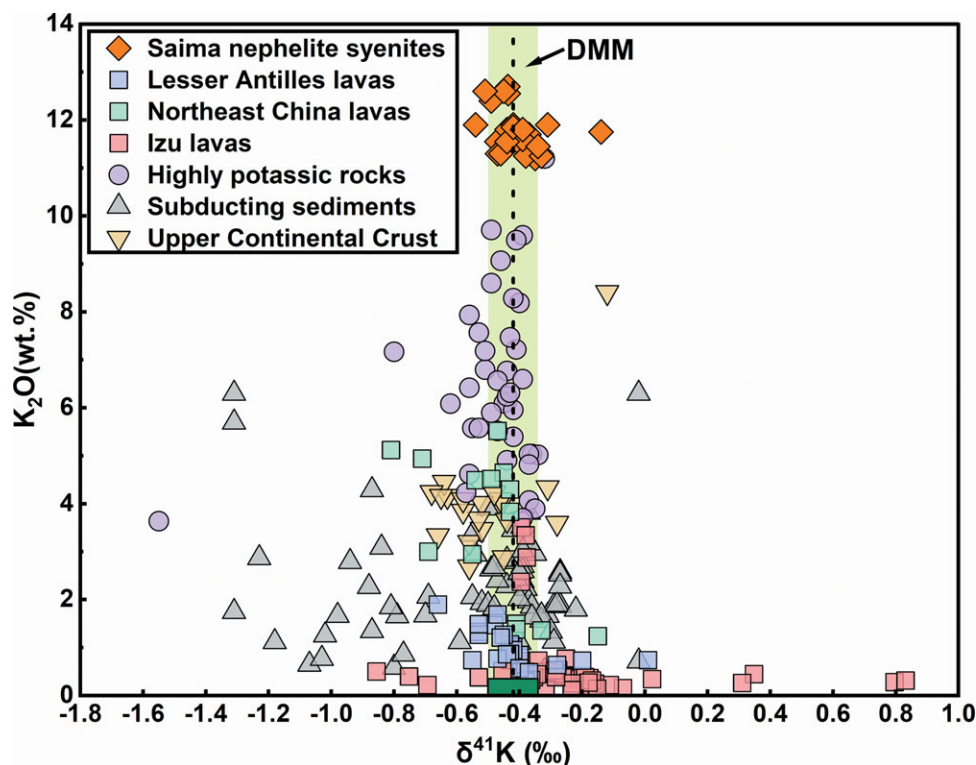
Fig. 1. (Colour online) K_2O versus $\delta^{41}K$ for the Saima nephelite syenites from the northeastern North China Craton. The data for subducting sediments, island arc lavas and orogenic high-potassic rocks are from Sun *et al.* (2020), Hu *et al.* (2021*a,b*), Wang, Z.-Z. *et al.* (2021) and Parendo *et al.* (2022). The K isotopic composition of the upper continental crust varies from −0.68 ‰ to −0.12 ‰, with an average of −0.44 ± 0.05 ‰ (Huang *et al.* 2020). The K isotopic compositions of fresh ocean island basalts are used to represent depleted mantle (depleted MORB mantle (DMM): $\delta^{41}K = -0.42 \pm 0.08$ ‰ (Hu *et al.* 2021*b*); $K_2O = 0.006$ % (Workman & Hart, 2005)).

CO_2, carbonate, H_2O and hydroxyl) were produced by the partial melting of the lithospheric mantle root, which was metasomatized by K-rich melts in the ancient subduction process. Such carbon and hydrogen oxides strongly influence the stability of partial melts in the lithospheric mantle root (Dasgupta *et al.* 2022). To evaluate the impact of chemical diffusion between these melts on the K–Sr–Nd isotopic compositions of the melts, and provide further indications for the decoupling of K isotopes from Sr–Nd isotopic compositions in the Saima alkaline complex, the diffusion model of K–Sr–Nd in the interactions of the cratonic roots and asthenosphere was simulated. The detailed modelling method is described below.

In the numerical simulation, diffusion coefficients were calculated using experimental data from Behrens & Hahn (2009) with a mantle potential temperature of 1280 °C for Sr and Nd, assuming that the temporal lithospheric thickness is 80 km and diffusion coefficient of K is three times that of Sr based on the compilations of Zhang *et al.* (2010). The calculation yields $D^K = 3.53 \times 10^{-10}$ m^2/s, $D^{Sr} = 1.17 \times 10^{-10}$ m^2/s and $D^{Nd} = 1.62 \times 10^{-11}$ m^2/s (for other parameters, see online Supplementary Material Table S4). Diffusion models of K–Sr–Nd were calculated based on Fick's second law and the conservation of mass in a convection system (Zhang, 2008). For the Sr–Nd radioactive decay system, the radioactive decay law was also considered. The interstitial melts in these two interacting reservoirs were chemically equilibrated with peridotites. We only considered the isotopic evolution of the MLMR as a result of chemical diffusion or radioactive decay with the asthenosphere and neglected the variations in element concentrations caused by diffusion. In addition, the MLMR is more volatile rich than the asthenosphere, and the diffusion of K, Sr and Nd in the MLMR is much faster than in the asthenosphere. Thus, the diffusive isotopic flux from the asthenosphere can be homogenized via diffusion over a finite time interval, i.e. the MLMR can be treated as an isotopically uniform system.

Based on the above discussion, there are interactions between the interstitial melts, from the MLMR and asthenosphere reservoirs, caused by chemical diffusion. The chemical evolution of the MLMR as a result of chemical diffusion with the asthenosphere can be described using the following equation:

$$\frac{\partial C}{\partial t} = D\frac{\partial^2 C}{\partial x^2} + v\frac{\partial C}{\partial x} \tag{1}$$

where C is the element concentration, t is the time, x is the distance, D is the diffusivity of the element in the interstitial melt and v is the plate velocity or convective velocity of the asthenosphere. We neglected the variations in element concentrations caused by diffusion and only considered the evolution of the isotope ratios. According to isotope exchange experiments (Baker, 1989; Lesher, 1990; van der Laan *et al.* 1994), the evolution of the isotopic ratio of the MLMR can be calculated using Equation (1) (Zhang, 2008); thus, the isotopic evolution of the system can be expressed as:

$$\frac{\partial R}{\partial t} = D\frac{\partial^2 R}{\partial x^2} + v\frac{\partial R}{\partial x} + I \tag{2}$$

where R is the isotopic ratio or isotope per mil variation δ, and the third term I on the right-hand side of Equation (2) represents the isotopic variation owing to radioactive decay. For the ^{147}Sm–^{143}Nd system, the $^{143}Nd/^{144}Nd$ variation due to ^{147}Sm decay to ^{143}Nd after time t can be calculated using Equation (3):

$$I = \frac{^{143}Nd}{^{144}Nd} - \left(\frac{^{143}Nd}{^{144}Nd}\right)_0 = \frac{^{147}Sm}{^{144}Nd}(e^{\lambda t} - 1) \tag{3}$$

where $^{143}Nd/^{144}Nd$ is the present isotopic ratio, $(^{143}Nd/^{144}Nd)_0$ is the initial isotopic ratio, $^{147}Sm/^{144}Nd$ is the parent–daughter ratio
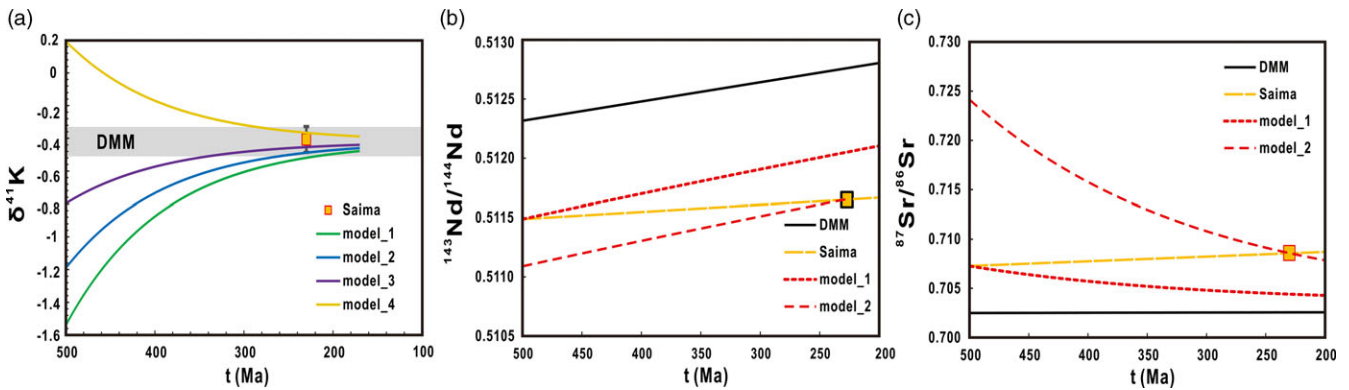
Fig. 2. (Colour online) Simulation calculation diagrams of K–Sr–Nd isotopes for the Saima alkaline rocks from the northeastern North China Craton. (a) Diffusion model diagram of K isotopes. The yellow box corresponds to the isotope ratios of the Saima alkaline rocks. (b, c) Diffusion model diagrams of Sr–Nd isotopes. Depleted MORB mantle (DMM) represents the isotope radioactive decay system of the asthenosphere data from Workman & Hart (2005). Model_1 represents the isotopic evolution of the MLMR as the result of radioactive decay, taking 0.707285 and 0.511487 as the initial values of $^{87}Sr/^{86}Sr$ and $^{143}Nd/^{144}Nd$ at 500 Ma, respectively. Model_2 represents the isotopic evolution of the MLMR as a result of chemical diffusion and radioactive decay, and the reset initial values are 0.72415 and 0.51109 by repeating the calculation, respectively. Nd isotope data of Saima alkaline complex from this study, Zhu *et al.* (2016) and Yang *et al.* (2005).

at time t and λ is the decay constant. The isotopic evolution of the MLMR and solutions of Equation (2) can be calculated using numerical methods. However, if we neglect the diffusive flux between the metasomatized and unmetasomatized lithospheric mantle, the isotopic flux J from the asthenosphere can be approximately expressed by Equation (4) (Mungall, 2002),

$$J = \frac{3\sqrt{2}}{4}(R_a - R_m)\rho_a\sqrt{\frac{D\upsilon}{X}} \qquad (4)$$

where ρ_a is the density of the asthenosphere and X is the characteristic length of the MLMR. R_a and R_m are the isotopic ratios of the asthenosphere and the MLMR, respectively. Note that R_a and R_m vary with time for radioactive decay systems such as the ^{147}Sm–^{143}Nd and ^{87}Rb–^{87}Sr systems. For a nonradioactive system, such as K isotopes, R_a is a constant, while R_m also varies with time owing to the flux from the convective asthenosphere. As mentioned above, the MLMR was more volatile rich than the asthenosphere, and the diffusions of K, Sr and Nd in the MLMR were much faster than those in the asthenosphere; thus, the diffusive isotopic flux from the asthenosphere can be homogenized by diffusion in a finite time interval, Δt; hence, R_m can be considered a constant within Δt.

If the initial K isotopic composition of the MLMR, R^0_m, is set as a random value between −1.55 ‰ and +0.2 ‰ (the range of K isotopic compositions of orogenic high-potassic rocks and island arc lavas), R^1_m of the MLMR after the first time step Δt can be calculated by

$$R^1_m = R^0_m + \frac{J\Delta t}{M_m} = R^0_m + \frac{3\sqrt{2}}{4V}(R_a - R^0_m)\sqrt{\frac{D\upsilon\Delta t^2}{X}} \qquad (5)$$

where V is the volume of the MLMR expressed as $V = M_m/\rho_m$, and M_m and ρ_m are the mass and density of the MLMR, respectively.

At the next time step, R^1_m is reset as the initial isotopic composition, and then R^2_m can be calculated as

$$R^2_m = R^1_m + \frac{J\Delta t}{M_m} = R^1_m + \frac{3\sqrt{2}}{4V}(R_a - R^1_m)\sqrt{\frac{D\upsilon\Delta t^2}{X}} \qquad (6)$$

By repeating the calculations using Equations (5–6), the entire K isotopic evolution of the MLMR can be evaluated.

If the metasomatism of the MLMR was t_m years ago for the ^{147}Sm–^{143}Nd system, then the $^{143}Nd/^{144}Nd$ ratios of the MLMR and asthenosphere at t_m are the initial compositions, denoted as R^0_m and R^0_a, respectively, and can be calculated using Equation (3). Thus, the R^1_m of the MLMR after the first time step Δt can be calculated as follows:

$$R^1_m = R^0_m + \frac{J\Delta t}{M_m} + I_1$$
$$= R^0_m + \frac{3\sqrt{2}}{4V}(R^0_a - R^0_m)\sqrt{\frac{D\upsilon\Delta t^2}{X}} + \left(\frac{^{147}Sm}{^{144}Nd}\right)_m(e^{\lambda\Delta t} - 1) \qquad (7)$$

where $(^{147}Sm/^{144}Nd)_m$ is the parent–daughter ratio of the MLMR and I_1 is the ingrowth due to radioactive decay after Δt.

In the next time step, R^1_a can be calculated by

$$R^1_a = \left(\frac{^{147}Sm}{^{144}Nd}\right)_a(e^{\lambda\Delta t} - 1) \qquad (8)$$

where $(^{147}Sm/^{144}Nd)_a$ is the parent–daughter ratio of the asthenosphere. R^1_m is reset as the initial isotopic composition and R^2_m can be calculated as

$$R^2 = R^1_m + \frac{J\Delta t}{M_m} + I_2$$
$$= R^1_m + \frac{3\sqrt{2}}{4V}(R^1_a - R^1_m)\sqrt{\frac{D\upsilon\Delta t^2}{X}} + \left(\frac{^{147}Sm}{^{144}Nd}\right)_m(e^{\lambda\Delta t} - 1) \qquad (9)$$

By repeating the calculations using Equations (7–9), the entire Nd isotopic evolution of the MLMR can be evaluated. Similarly, other radioactive isotopic systems of MLMRs, such as Sr, can also be evaluated.

The simulation results were obtained through the above process. For the nonradioactive system (Fig. 2a), with the chemical diffusion of K between interstitial melts from the MLMR and asthenosphere, K isotopic compositions with sediment signals of the MLMR tended to be in equilibrium with the
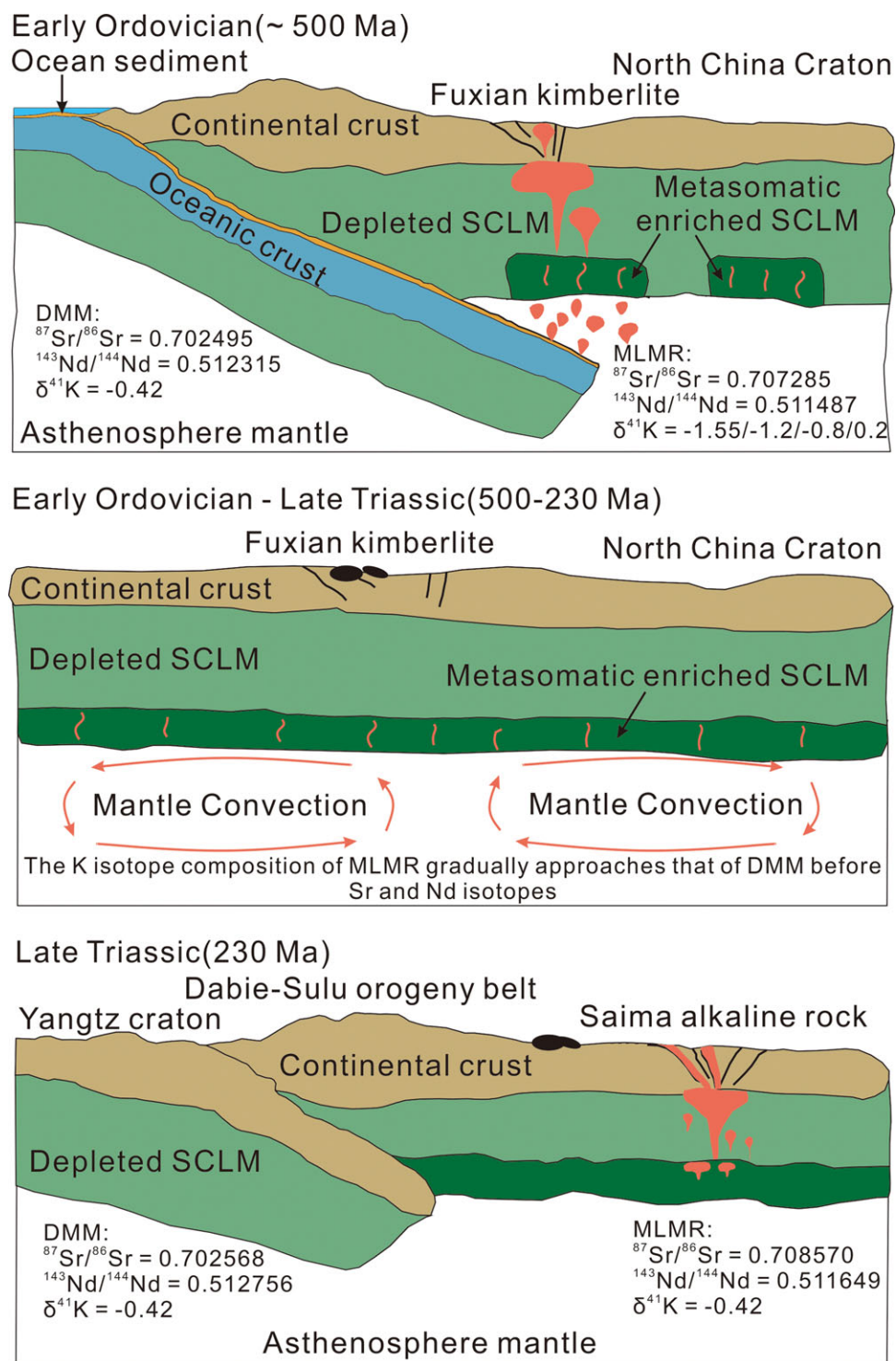
Fig. 3. (Colour online) Schematic diagram of the petrogenesis of the Saima alkaline rocks from the northeastern North China Craton. The Fuxian kimberlites are used to represent the initial formation of the metasomatized lithospheric mantle in the Saima alkaline rock source area in early Ordovician time (~500 Ma). SCLM – sub-continental lithospheric mantle.

asthenosphere at 230 Ma, consistent with the present K isotopic composition of the Saima alkaline rocks. Compared with the K isotopic data for orogenic high-potassic rocks and island arc lavas (−1.55 ‰ to +0.2 ‰) (Fig. 2), the nearly identical K isotopic compositions for the Saima and asthenospheric mantles are low probability events (<10 %). For the Sr–Nd radioactive decay system (Fig. 2b, c), the Sr–Nd isotope ratios of the MLMR cannot evolve into the isotope ratio values of the Saima alkaline rocks at 230 Ma based on Model_1. Other processes are required for the isotopic evolution of the MLMR.

Through the processes of radioactive decay and chemical diffusion (Model_2), the Sr–Nd isotope system of the MLMR could evolve to the ratios of the Saima alkaline rocks at 230 Ma. Therefore, because of the faster diffusion rate of K than that of Sr and Nd, the Sr–Nd isotope system could preserve the signals of both the mantle and crust, while the K isotopes only reflect the characteristics of the asthenospheric mantle.

In our numerical simulations, the variations of elements are not considered since isotope exchange by diffusion is much greater than element exchange (Zhang, 2008), according to

isotope exchange experiments (Baker, 1989; Lesher, 1990; van der Laan *et al.* 1994). Moreover, the element concentrations of interest in the Saima source region are not well constrained. In addition, the time required to homogenize the isotopic composition of the MLMR highly depends on the size of the MLMR and the diffusivities of elements, which in turn depends on the temperature. Assuming that the temporal lithospheric thickness was 200 km 500 Ma ago, the actual temperature at the LAB was 1380 °C, and the diffusivity of the isotopic element is three times that of the element; thus, the calculated time to homogenize the K isotopic composition of the MLMR is less than 100 Myrs with other parameters fixed. This exercise demonstrates our model is robust and reasonable although many parameters are not well constrained. The above results show that the K isotopic composition of this particular size MLMR is gradually homogenized under mantle convection within a certain time span. However, although mantle convection can reduce mantle heterogeneity to some extent, the mantle still has heterogeneity at different scales from thousands of kilometres to several centimetres (Kogiso *et al.* 2004; Huang & Davies, 2007; Iwamori & Nakamura, 2015).

Besides K, He, H and Li are also fast-diffusion components, and their diffusivities are higher than that of K in the silicate melts or solid mantle (Sun *et al.* 2015; Wang *et al.* 2015; Demouchy & Bolfan-Casanova, 2016). According to our model, identical He, H and Li isotopic compositions to the asthenospheric mantle in the Saima alkaline complex are therefore expected. However, these isotopic systems are more sensitive to crustal contamination (Hilton & Porcelli, 2014) and diffusion-driven isotopic fractionation after intrusion into wall rocks (Teng *et al.* 2006); thus, their original asthenospheric signatures cannot be easily preserved.

4. Conclusions

This research provides examples of the decoupling of K isotopes and Sr–Nd isotopes when the interaction of MLMR and asthenosphere is rate-limited by diffusion. The numerical simulations reproduced the K–Sr–Nd isotopic compositions of the Saima alkaline complex if its source area was modified before 500 Ma. In early Palaeozoic time (~500 Ma), the sub-continental lithospheric mantle of the eastern NCC was metasomatized by subducted sediment-derived melt (Fig. 3). The continuous interaction of the metasomatized lithospheric mantle and convective asthenosphere by chemical diffusion of interstitial melts resulted in homogenized K isotopic compositions in these two reservoirs before ~230 Ma, from which the Saima alkaline rocks formed. The Sr–Nd isotope system of the metasomatized lithospheric mantle still records the original signatures because of its long radioactive half-life and slow diffusion. Our data confirm the elimination of K isotopic heterogeneity by mantle convection in the Saima mantle source, and it highlights the role of the size of the MLMR and the diffusion rate of the element in determining the composition of the MLMR.

References

Baker DR (1989) Tracer versus trace element diffusion: diffusional decoupling of Sr concentration from Sr isotopic composition. *Geochimica et Cosmochimica Acta* **53**, 3015–23.

Behrens H and Hahn M (2009) Trace element diffusion and viscous flow in potassium-rich trachytic and phonolitic melts. *Chemical Geology* **259**, 63–77.

Dasgupta R, Chowdhury P, Eguchi J, Eguchi J, Sun C and Saha S (2022) Volatile-bearing partial melts in the lithospheric and sub-lithospheric mantle on Earth and other rocky planets. *Reviews in Mineralogy and Geochemistry* **87**, 575–606.

Debayle E, Bodin T, Durand S and Ricard Y (2020) Seismic evidence for partial melt below tectonic plates. *Nature* **586**, 555–9.

Demouchy S and Bolfan-Casanova N (2016) Distribution and transport of hydrogen in the lithospheric mantle: a review. *Lithos* **240–243**, 402–25.

Foley SF, Venturelli G, Green DH and Toscani L (1987) The ultrapotassic rocks – characteristics, classification, and constraints for petrogenetic models. *Earth-Science Reviews* **24**, 81–134.

Hawkesworth CJ and Vollmer R (1979) Crustal contamination versus enriched mantle: $^{143}Nd/^{144}Nd$ and $^{87}Sr/^{86}Sr$ evidence from the Italian volcanics. *Contributions to Mineralogy and Petrology* **69**, 151–65.

Hilton DR and Porcelli D (2014) Noble gases as mantle tracers. In *Treatise on Geochemistry, Second Edition, Volume 3* (eds HD Holland and KK Turekian), pp. 293–325. Oxford: Elsevier.

Hu Y, Chen XY, Xu Y-K and Teng F-Z (2018) High-precision analysis of potassium isotopes by HR-MC-ICPMS. *Chemical Geology* **493**, 100–8.

Hu Y, Teng FZ and Chauvel C (2021a) Potassium isotopic evidence for sedimentary input to the mantle source of Lesser Antilles lavas. *Geochimica et Cosmochimica Acta* **295**, 98–111.

Hu Y, Teng FZ, Helz RT and Chauvel C (2021b) Potassium isotope fractionation during magmatic differentiation and the composition of the mantle. *Journal of Geophysical Research: Solid Earth* **126**, e2020JB021543. doi: 10.1029/2020JB021543

Huang J and Davies GF (2007) Stirring in three-dimensional mantle convection models and implications for geochemistry: passive tracers. *Geochemistry, Geophysics, Geosystems* **8**, Q03017. doi: 10.1029/2006GC001312.

Huang TY, Teng FZ, Rudnick RL, Chen XY, Hu Y, Liu YS and Wu FY (2020) Heterogeneous potassium isotopic composition of the upper continental crust. *Geochimica et Cosmochimica Acta* **278**, 122–36.

Iwamori H and Nakamura H (2015) Isotopic heterogeneity of oceanic, arc and continental basalts and its implications for mantle dynamics. *Gondwana Research* **27**, 1131–52.

Jahn BM, Wu FY, Lo CH and Tsai CH (1999) Crust-mantle interaction induced by deep subduction of the continental crust: geochemical and Sr-Nd isotopic evidence from post-collisional mafic-ultramafic intrusions of the northern Dabie complex, central China. *Chemical Geology* **157**, 119–46.

Kawakatsu H, Kumar P, Takei Y, Shinohara M, Kanazawa T, Araki E and Suyehiro K (2009) Seismic evidence for sharp lithosphere-asthenosphere boundaries of oceanic plates. *Science* **324**, 499–502.

Kogiso T, Hirschmann MM and Reiners PW (2004) Length scales of mantle heterogeneities and their relationship to ocean island basalt geochemistry. *Geochimica et Cosmochimica Acta* **68**, 345–60.

Lasaga AC (1998) *Kinetic Theory in the Earth Sciences*. Princeton: Princeton University Press.

Lesher CE (1990) Decoupling of chemical and isotopic exchange during magma mixing. *Nature* **344**, 235–7.

McKenzie D (1989) Some remarks on the movement of small melt fractions in the mantle. *Earth and Planetary Science Letters* **95**, 53–72.

Mungall JE (2002) Kinetic controls on the partitioning of trace elements between silicate and sulfide liquids. *Journal of Petrology* **43**, 749–68.

Naif S, Key K, Constable S and Evans RL (2013) Melt-rich channel observed at the lithosphere-asthenosphere boundary. *Nature* **495**, 356–9.

Parendo CA, Jacobsen SB, Kimura JI and Taylor RN (2022) Across-arc variations in K-isotope ratios in lavas of the Izu arc: evidence for progressive depletion of the slab in K and similarly mobile elements. *Earth and Planetary Science Letters* **578**, 117291. doi: 10.1016/j.epsl.2021.117291

Platzner IT (1997) *Modern Isotope Ratio Mass Spectrometry.* Chichester: Wiley.

Rudnick RL and Gao S (2014) Composition of the Continental Crust. In *Treatise on Geochemistry, Second Edition* (eds HD Holland and KK Turekian), pp. 1–51. Oxford: Elsevier.

Rychert CA, Tharimena S, Harmon N, Wang S, Constable S, Kendall JM, Bogiatzis P, Agius MR and Schlaphorst D (2021) A dynamic lithosphere–asthenosphere boundary near the equatorial Mid-Atlantic Ridge. *Earth and Planetary Science Letters* **566**, 116949. doi: 10.1016/j.epsl.2021.116949

Sun SS and McDonough WF (1989) Chemical and isotopic systematics of oceanic basalts: implications for mantle composition and processes. *Geological Society, London, Special Publications* **42**, 313–45.

Sun W, Yoshino T, Sakamoto N and Yurimoto H (2015) Hydrogen self-diffusivity in single crystal ringwoodite: implications for water content and distribution in the mantle transition zone. *Geophysical Research Letters* **42**, 6582–9.

Sun Y, Teng FZ, Hu Y, Chen XY and Pang KN (2020) Tracing subducted oceanic slabs in the mantle by using potassium isotopes. *Geochimica et Cosmochimica Acta* **278**, 353–60.

Teng F-Z, McDonough WF, Rudnick RL and Walker RJ (2006) Diffusion-driven extreme lithium isotopic fractionation in country rocks of the Tin Mountain pegmatite. *Earth and Planetary Science Letters* **243**, 701–10.

van der Laan S, Zhang Y, Kennedy AK and Wyllie PJ (1994) Comparison of element and isotope diffusion of K and Ca in multicomponent silicate melts. *Earth and Planetary Science Letters* **123**, 155–66.

Wang K, Brodholt J and Lu X (2015) Helium diffusion in olivine based on first principles calculations. *Geochimica et Cosmochimica Acta* **156**, 145–53.

Wang K, Li WQ, Li SL, Tian Z, Koefoed P and Zheng XY (2021) Geochemistry and cosmochemistry of potassium stable isotopes. *Geochemistry* **81**, 125786. doi: 10.1016/j.chemer.2021.125786

Wang Z-Z, Teng F-Z, Prelević D, Liu S-A and Zhao Z (2021) Potassium isotope evidence for sediment recycling into the orogenic lithospheric mantle. *Geochemical Perspectives Letters* **18**, 43–7.

Workman RK and Hart SR (2005) Major and trace element composition of the depleted MORB mantle (DMM). *Earth and Planetary Science Letters* **231**, 53–72.

Xu Y-K, Hu Y, Chen X-Y, Huang T-Y, Sletten RS, Zhu D and Teng F-Z (2019) Potassium isotopic compositions of international geological reference materials. *Chemical Geology* **513**, 101–7.

Yang JH, Chung SL, Wilde SA, Wu FY, Chu MF, Lo CH and Fan HR (2005) Petrogenesis of post-orogenic syenites in the Sulu Orogenic Belt, East China: geochronological, geochemical and Nd-Sr isotopic evidence. *Chemical Geology* **214**(1–2), 99–125.

Zhang HF and Yang YH (2007) Emplacement age and Sr-Nd-Hf isotopic characteristics of the diamondiferous kimberlites from the eastern North China Craton. *Acta Petrologica Sinica* **23**, 285–94.

Zhang Y (2008) *Geochemical Kinetics.* Princeton: Princeton University Press.

Zhang Y, Ni H and Chen Y (2010) Diffusion data in silicate melts. *Reviews in Mineralogy and Geochemistry* **72**, 311–408.

Zhu YS, Yang JH, Sun JF and Wang H (2017) Zircon Hf-O isotope evidence for recycled oceanic and continental crust in the sources of alkaline rocks. *Geology* **45**, 407–10.

Zhu YS, Yang JH, Sun JF, Zhang JH and Wu FY (2016) Petrogenesis of coeval silica-saturated and silica-undersaturated alkaline rocks: mineralogical and geochemical evidence from the Saima alkaline complex, NE China. *Journal of Asian Earth Sciences* **117**, 184–207.